


## Magnetism and magnetic anisotropy in $Nb_3Cl_8$ revealed by electron spin resonance

Ubaid Raza, Zhijie Ma(马之杰), Fangwei Wang(王芳卫), Youguo Shi(石友国), Lunhua He(何伦华), and Liqin Yan(闫丽琴)

**Citation:**Chin. Phys. B, 2026, 35 (**5**): 057601. DOI: 10.1088/1674-1056/ae194e
http://cpb.iphy.ac.cn; http://iopscience.iop.org/cpb

**What follows is a list of articles you may be interested in**

---

## Low-energy spin dynamics in a Kitaev material $Na_3Ni_2BiO_6$ investigated by nuclear magnetic resonance

Xinyu Shi(史昕雨), Yi Cui(崔祎), Yanyan Shangguan(上官艳艳), Xiaoyu Xu(徐霄宇), Zhanlong Wu(吴占龙), Ze Hu(胡泽), Shuo Li(李硕), Kefan Du(杜柯帆), Ying Chen(陈颖), Long Ma(马龙), Zhengxin Liu(刘正鑫), Jinsheng Wen(温锦生), Jinshan Zhang(张金珊), and Weiqiang Yu(于伟强)
Chin. Phys. B, 2024, 33 (**6**): 067601. DOI: 10.1088/1674-1056/ad3dce

## A low-noise X-band microwave source with digital automatic frequency control for electron paramagnetic resonance spectroscopy

Yu He(贺羽), Runqi Kang(康润琪), Zhifu Shi(石致富), and Xing Rong(荣星)
Chin. Phys. B, 2023, 32 (**8**): 087601. DOI: 10.1088/1674-1056/accf7e

## A design of resonant cavity with an improved coupling-adjusting mechanism for the W-band EPR spectrometer

Yu He(贺羽), Runqi Kang(康润琪), Zhifu Shi(石致富), Xing Rong(荣星), and Jiangfeng Du(杜江峰)
Chin. Phys. B, 2022, 31 (**11**): 117601. DOI: 10.1088/1674-1056/ac7bfd

## Determination of charge-compensated $C_{3v}$ (II) centers for $Er^{3+}$ ions in $CdF_2$ and $CaF_2$ crystals

Rui-Peng Chai(柴瑞鹏), Dan-Hui Hao(郝丹辉), Dang-Li Gao(高当丽), and Qing Pang(庞庆)
Chin. Phys. B, 2021, 30 (**3**): 037601. DOI: 10.1088/1674-1056/abc3b0

## Covalent bonding and *J-J* mixing effects on the EPR parameters of $Er^{3+}$ ions in GaN crystal

Rui-Peng Chai(柴瑞鹏), Long Li(李隆), Liang Liang(梁良), Qing Pang(庞庆)
Chin. Phys. B, 2016, 25 (**7**): 077601. DOI: 10.1088/1674-1056/25/7/077601

---

# Magnetism and magnetic anisotropy in $Nb_3Cl_8$ revealed by electron spin resonance

Ubaid Raza[1,2], Zhijie Ma(马之杰)[1], Fangwei Wang(王芳卫)[1,2], Youguo Shi(石友国)[1], Lunhua He(何伦华)[1,2], and Liqin Yan(闫丽琴)[1,2,†]

[1] *Beijing National Laboratory for Condensed Matter Physics, Institute of Physics, Chinese Academy of Sciences, Beijing* 100190, *China*
[2] *School of Physical Sciences, University of Chinese Academy of Sciences, Beijing* 100190, *China*

(Received 4 August 2025; revised manuscript received 17 October 2025; accepted manuscript online 30 October 2025)

This study investigates the microscopic spin dynamics and anisotropic magnetic behavior in van der Waals kagome magnet $Nb_3Cl_8$ by employing electron spin resonance (ESR) spectroscopy on both powder and single-crystal samples over the temperature range of 5 K–300 K. The effective $g$, peak to peak linewidths ($\Delta H_{pp}$), and double integrated intensities ($I$) were extracted from the ESR spectra to analyze the temperature-dependent evolution of spin–orbit coupling and spin–spin interactions. The formation of singlet ground state in single crystal $Nb_3Cl_8$ at $T^* \sim 100$ K is observed, evidenced by the maximum $\Delta H_{pp}$ and $g$ at $T^*$, along with the decrease in intensity $I$, which is consistent to the reported non-magnetic transition in the single-crystal $Nb_3Cl_8$. Moreover, the spectral difference between $H \parallel c$ and $H \perp c$ configurations imply subtle magnetic anisotropy in single crystal $Nb_3Cl_8$. However, there is no non-magnetic transition was observed in powder $Nb_3Cl_8$ since the parameters of $\Delta H_{pp}$ and $I$ keep stable at $T^*$. It might be attributed to the grain averaging and random orientation effects. Our study provides valuable insights into the magnetic interplay in $Nb_3Cl_8$ and prove the potential of ESR spectroscopy as a powerful tool for probing the intrinsic magnetism.

**Keywords:** $Nb_3Cl_8$, ESR spectroscopy, spin dynamics, magnetic anisotropy

**PACS:** 76.30.–v, 71.70.Ej, 76.60.Es, 75.30.Gw

**DOI:** 10.1088/1674-1056/ae194e **CSTR:** 32038.14.CPB.ae194e

## 1. Introduction

Recently, two-dimensional (2D) materials have attracted much attention owing to their electronic, magnetic and mechanical properties that are distinctly different from the bulk of the same.[1,2] These materials have been studied and it has been discovered that they are hosts for new quantum phases such as topological flat bands, quantum spin liquid state and Mott insulators each essential for quantum computing, spintronics, and tunable magnetic systems.[3] Among some of these various 2D materials, van der Waals (vdW) compounds, with weak intra and inter layer coupling, strong intra layer bonding, have emerged as perhaps the most promising candidates for future next generation quantum technologies.[4] $Nb_3Cl_8$, a member of the vdW family, has been of interest due to its kagome lattice structure formed by $Nb_3$ trimers, as depicted in Fig. 1(a). The magnetic behavior of the material is fundamentally governed by these $Nb_3$ trimers, which host magnetic moments arising from unpaired electrons.[5] $Nb_3Cl_8$ undergoes a transition from a paramagnetic state at high temperature to a non-magnetic singlet ground state at $T^* \sim 100$ K. The charge disproportionation is thought to drive this transition, which originated from structural rearrangements of $Nb_3$ trimer resulting in the formation of nonmagnetic $[Nb_3]^{7+}$ and $[Nb_3]^{9+}$ species,[6] and thus changing the overall magnetic state of the compound, as shown in Figs. 1(b) and 1(c).

Much work has been performed on understanding the complex magnetism and origin of different quantum phases in $Nb_3Cl_8$, such as NMR, VSM, temperature-dependent magnetic susceptibility, STEM, ARPES, specific heat capacity, electrical conductivity, and first principles calculations.[5–14] However, less work has focused on the understanding of the spin–spin interactions, spin–orbit coupling, tiny changes in local magnetic environment during transition temperature $T^*$ and magnetic anisotropy in $Nb_3Cl_8$.

Electron spin resonance spectroscopy (ESR) is a very powerful technique to probe magnetic interactions at the microscopic level.[15] The peak-to-peak line width, $H_{pp}$, observed in the ESR signal is directly associated with the interactions of the spins with their environment.[16] The double integrated intensity $I(T)$ reflects the spin density.[17] The $g$-factor, extracted from the resonance line, indicates the strength of the spin–orbit coupling.[18] In this work, we used ESR spectroscopy on powder and single crystal samples of $Nb_3Cl_8$ over the temperature range of 5 K–300 K, and measurements on single crystals were conducted with the $H$ parallel and perpendicular to the $c$ axis. The temperature-induced changes in ESR parameters (the $g$, $\Delta H_{pp}$, and intensity $I$) provide a deeper understanding of the non-magnetic phase transition of $Nb_3Cl_8$. The anisotropy of spin–orbit coupling, exchange interactions and spin lattice relaxation dynamics are studied by comparing the behaviors of powder $Nb_3Cl_8$ and single crystal $Nb_3Cl_8$ under both $H \parallel c$-axis and $H \perp c$-axis geometries.

†Corresponding author. E-mail: lqyan@iphy.ac.cn

© 2026 Chinese Physical Society and IOP Publishing Ltd. All rights, including for text and data mining, AI training, and similar technologies, are reserved.

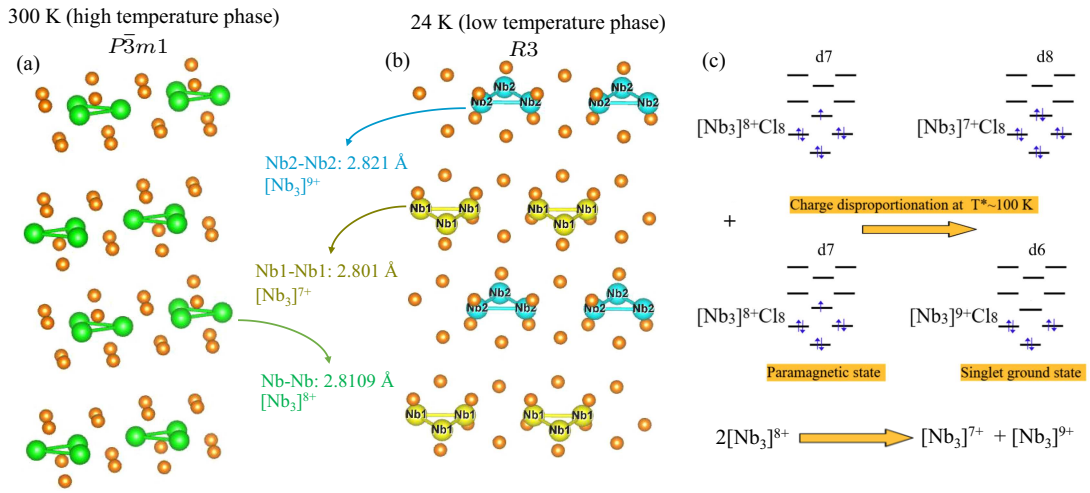



**Fig. 1.** (a) Crystal structure of $Nb_3Cl_8$ in high temperature $P\bar{3}m1$ phase, showing $Nb_3$ trimmer with uniform Nb–Nb bond length. (b) Low temperature $R3$ phase showing charge disproportionated non-magnetic $Nb_3$ clusters with different bond lengths. (c) Schematic showing electronic level filling and transition from paramagnetic to singlet ground state at $T^* = 100$ K.

## 2. Experiment

### 2.1. Sample preparation and characterization

Powders of $NbCl_5$ and elemental Nb served as the starting materials. The precursor was synthesized by mixing these materials in a molar ratio of Nb:Cl = 3:8 and calcining the mixture in a sealed silica tube under an argon atmosphere at 700 °C for 48 hours. Subsequently, single crystals of $Nb_3Cl_8$ were grown from the precursor powders using a $PbCl_2$ flux method via solvent evaporation at 750 °C for 150 hours. After crystal growth, any residual $PbCl_2$ was removed by soaking the crystals in hot water. Finally, powder samples of $Nb_3Cl_8$ were prepared by grinding the as-grown single crystals, a method chosen to prevent chemical decomposition that can occur during mechanical grinding.[6] The single crystal sample has been characterized using single crystal x-ray diffractometer (XRD). The scanning electron microscopy (SEM), and energy-dispersive x-ray spectroscopy (EDS) were employed using Regulus 8230, Manufacturer: Hitachi, Japan.

### 2.2. ESR measurements

ESR measurements were performed using a JEOL JES-FA200 spectrometer operating at x-band frequencies (∼9.3 GHz) at selected temperatures from 5 K to 300 K. The experiments were conducted at a microwave power of 1 mW, including single crystal with the magnetic field oriented both parallel and perpendicular to the $c$-axis, as well as powder $Nb_3Cl_8$. The temperature dependence of $g$ obtained from the peak of ESR spectra calculated by resonance condition $h\upsilon = g\mu_B H_r$ over the temperature range of 5 K–300 K. The peak-to-peak line width $\Delta H_{pp}$, calculated by the $H$ distance recorded between the maximum and minimum peaks of first derivative ESR spectra $dP/dH$ using the formula $\Delta H_{pp} = H_{max} - H_{min}$. The temperature dependence of intensity $I$, obtained from double integration of ESR spectra $dP/dH$. The $\Delta H_{pp}$ of the ESR signal was analyzed to elucidate interactions between the spins and their local environment. Additionally, the $I$ which is proportional to the number of unpaired electrons and the $g$ factor extracted from the resonance spectra provided valuable insights into the spin–orbit coupling.[15–20]

## 3. Results and discussion

Figure 2 presents the XRD spectrum measured along the (00$l$) direction, The sharp peaks indicate the phase purity and high quality of the crystal.

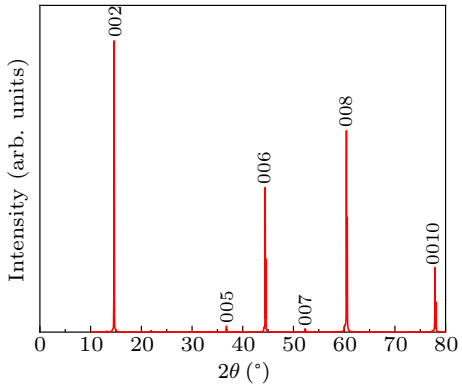



**Fig. 2.** The XRD pattern of the single crystal $Nb_3Cl_8$ measured along the 00$l$ direction. The Miller indices are indicated in the plot.

The surface morphology of the $Nb_3Cl_8$ single crystal was examined using scanning electron microscopy, as shown in Fig. 3(a). The crystal exhibits smooth, plate-like surfaces, characteristic of the lamellar structure associated with van der Waals-bonded 2D materials.[27] The uniform morphology and absence of visible microcracks indicate high crystallinity of the grown crystal.

The corresponding energy-dispersive x-ray spectroscopy (EDS) analysis, presented in Fig. 3(b), confirms the elemental composition of the sample. The quantified atomic ratio of Nb : Cl ≈ 1 : 2.7 is in close agreement with the 3 : 8 stoichio-

metric ratio of $Nb_3Cl_8$, thereby confirming the correct chemical composition and homogeneity of the synthesized single crystal.

Figure 4(a) presents the ESR spectra of single-crystal $Nb_3Cl_8$ measured with $H \parallel c$ at selected temperatures from 5 K to 300 K. At higher temperatures, the broader resonance lines with the $H$ center around 310 mT, which holds up to $T^*$, indicating weak spin–spin interactions in paramagnetic regime.[21] A subtle change in resonance field was observed at $T^*$ which are the onset of non-magnetic transition. This behavior is directly associated with charge disproportionation of $Nb_3$ trimers, which suppress the collective spin response and drive the system into a singlet ground state. $T^*$ corresponds to the reported temperature where non-magnetic transition appears.[6]

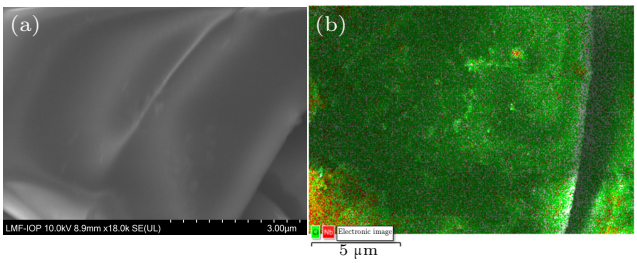



**Fig. 3.** (a) SEM image of single crystal $Nb_3Cl_8$, (b) EDS elemental mapping of single crystal sample.

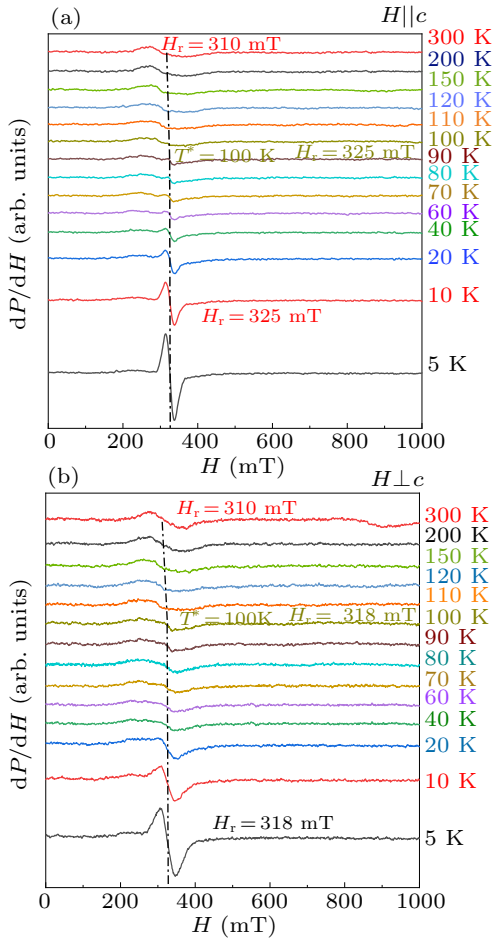



**Fig. 4.** The ESR spectra $dP/dH$ at selected temperatures from 5 K to 300 K for single crystal $Nb_3Cl_8$ with (a) $H \parallel c$ and (b) $H \perp c$.

Figure 4(b) shows the ESR spectra $dP/dH$ for single crystal $Nb_3Cl_8$ recorded with $H \perp c$, which exhibiting notable differences from the $H \parallel c$. It indicates the anisotropy of magnetic interactions in single crystal $Nb_3Cl_8$. Above $T^*$, the ESR spectra exhibits the resonance features similar to the one with $H \parallel c$, indicating the rapid spin lattice relaxation in paramagnetic regime.[21] Upon cooling below $T^*$, the ESR spectra remain significantly broader in entire temperature range as compared to $H \parallel c$ geometry. This comparative broadening implies more efficient energy transfer to the lattice, consistent with anisotropic exchange interactions, expected in layered transition metal halides.[18]

The temperature dependence of the intensity $I$, peak-to-peak line width $\Delta H_{pp}$ and $g$ calculated for $H \parallel c$ orientation are presented in Fig. 5(a). One can see in that $g$ is gradually increasing with decreasing temperature from 300 K and reaching a maximum at $T^*$, reflecting a progressive enhancement of spin–orbit coupling effects.[22] Whereas, the $\Delta H_{pp}$ remains nearly stable in this paramagnetic regime. As the temperature is further lowered below $T^*$, the $g$ and $\Delta H_{pp}$ decreases rapidly, signaling the changes in local crystal field, spin–orbit and spin–spin interactions,[18] since the emergence of electronic reordering between $[Nb_3]^{7+}$ and $[Nb_3]^{9+}$, happened with the decrease and increase of Nb–Nb bond length together.[8] The intensity $I$, which is proportional to the number of unpaired spins ($M$) contributing to the resonance, fully suppressed at $T^*$ with decreasing $T$. This suppression of $I$ at $T^*$ is indicating the loss of ESR active spins, confirmed the formation of singlet ground state. A sharp upturn in $I$, reduction in $g$ and relatively narrow $\Delta H_{pp}$ below 10 K suggesting the paramagnetic interactions among defect-induced spins;[24] while the overall state remains non-magnetic singlet spin state. This defect induced paramagnetic impurity has also been observed in previous magnetic susceptibility studies. These trends in $g$, $\Delta H_{pp}$ and $I$, are consistent to the reported non-magnetic transition in single crystal $Nb_3Cl_8$ at $T^*$.[5,6]

Figure 5(b) displays the temperature dependence of $g$, $\Delta H_{pp}$, and $I$ for single crystal of $Nb_3Cl_8$ measured with $H \perp c$. From 300 K to 100 K, the $g$ increases steadily and reaching maximum at $T^*$ with decreasing $T$, similar to the $H \parallel c$ orientation, suggesting the progressive enhancement of spin orbit coupling effect in paramagnetic state.[17] Simultaneously, the $\Delta H_{pp}$ exhibits the non-monotonic trend which differs with $H \parallel c$, implies anisotropy magnetic interactions in paramagnetic state. Below $T^*$, the rapid decrease in $g$ and $\Delta H_{pp}$, along with suppression of $I$, suggests the notable changes in local magnetic environment due to charge disproportionation. The small upturn in $\Delta H_{pp}$ and $g$ at 65 K, suggesting strong spin–spin and spin–orbit interactions among defect induced paramagnetic moments in non-magnetic matrix.

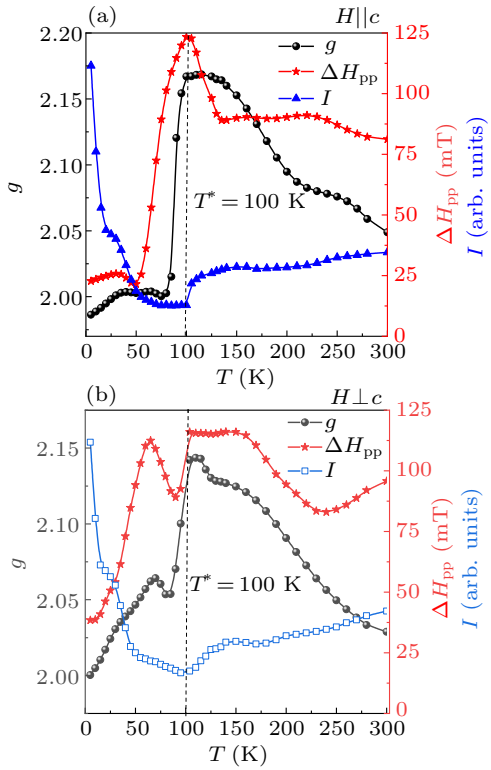



**Fig. 5.** (a)–(b) The temperature dependence of ESR parameters ($g$, line width $\Delta H_{pp}$, and intensity $I$) for single crystal of $Nb_3Cl_8$ with $H \parallel c$ $H \perp c$ respectively.

The previous magnetic susceptibility studies exhibit the orientation dependent anisotropy in single crystal $Nb_3Cl_8$.[6] In our single crystal ESR measurements, the temperature-dependent $g$-factor and line width ($\Delta H_{pp}$) exhibit clear anisotropy between the different $c$-axis orientations, consistent with literature. Kagome and cluster-based magnets often exhibit strong anisotropy and unconventional spin dynamics due to geometrical frustration and orbital effects.[26] However, in contrast to frustrated kagome antiferromagnets that retain fluctuating spins down to low temperature, $Nb_3Cl_8$ undergoes a complete transition into a non-magnetic singlet state due to charge ordering within $Nb_3$ clusters as shown in Figs. 1(a) and 1(b). This distinction highlights the unique mechanism of anisotropy in $Nb_3Cl_8$, which originates from cluster-level structural rearrangements rather than purely geometric frustration.

The derivative ESR spectra of powder $Nb_3Cl_8$ at selected temperatures from 5 K–300 K is presented in Fig. 6(a). From 300 K–20 K, the ESR spectra displays broader and less intense resonance lines, which implies paramagnetic (PM) state where $[Nb_3]^{8+}$ clusters exhibit weak spin–spin interactions and magnetic moments are largely uncorrelated.[17] As the temperature is further lowered to 10 K, there is single resonance line with Lorentzian line shape appears as the thermal agitations diminished, indicates the paramagnetic ordering over the entire temperature range from 5 K to 300 K in powder $Nb_3Cl_8$.

The temperature dependence of $\Delta H_{pp}$ and $I$ for powder $Nb_3Cl_8$ are presented in Fig. 6(b). The monotonic increase in $I$ at 300 K–5 K with decreasing $T$, reflects a typical Curie-type paramagnetic response, where thermal depopulation of excited states enhances spin polarization. This indicates that weakly interacting local magnetic moments persists throughout the measured temperature range. The $\Delta H_{pp}$ increases linearly from 300 K to 50 K with decreasing $T$, suggesting the growing spin–spin interactions and enhanced spin lattice relaxation in paramagnetic state.[16] Below 50 K, the $\Delta H_{pp}$ is narrowing rapidly, indicating the suppression in spin–spin interactions while the $I$ increases with decreasing $T$, which implies the presence of correlated paramagnetic state. These findings are consistent with previous literature on $Nb_3Cl_8$ powder, where no non-magnetic transition is observed.[8]

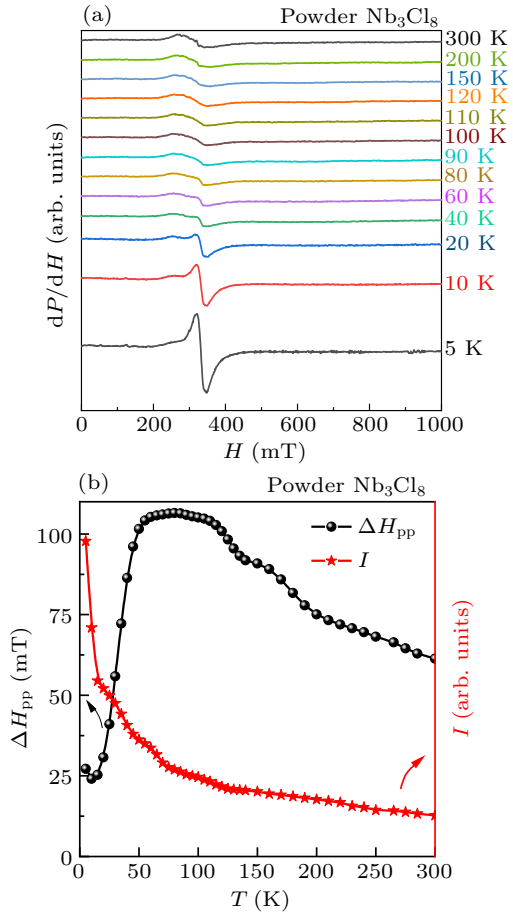



**Fig. 6.** (a) The ESR spectra $dP/dH$ at selected temperatures from 5 K to 300 K for powder of $Nb_3Cl_8$. (b) The temperature dependence of ESR parameters ($\Delta H_{pp}$ and $I$) for powder of $Nb_3Cl_8$.

Figures 7(a) and 7(b) present the comparisons of temperature dependence of $\Delta H_{pp}$ and $g$ of powder $Nb_3Cl_8$ and single crystal $Nb_3Cl_8$ with $H \parallel c$ and $H \perp c$, respectively. Together, these trends display how sample morphology (powder versus single crystal) and magnetic field orientation ($H \parallel c$ and $H \perp c$) influence the local magnetic environment in $Nb_3Cl_8$.

Figure 7(a) presents the temperature dependence of $\Delta H_{pp}$ for powder $Nb_3Cl_8$ and single crystal $Nb_3Cl_8$ with $H \parallel c$ and $H \perp c$. The subtle differences in $\Delta H_{pp}$ for both $H \parallel c$ and $H \perp c$ clearly indicating the anisotropic magnetic interactions in the

single crystal $Nb_3Cl_8$. The increase in $g$ around $T^*$ in powder $Nb_3Cl_8$ is more modest likely due to averaging of anisotropic effects. Figure 7(b) presents the $g$ trends for powder $Nb_3Cl_8$ and single crystal $Nb_3Cl_8$ with both $H \parallel c$ and $H \perp c$. The single crystal $Nb_3Cl_8$ exhibits pronounced broadening for both $H \parallel c$ and $H \perp c$ orientations with notable differences, which confirmed the anisotropic local magnetic environment. The powder $Nb_3Cl_8$ exhibits modest response likely due to grain averaging and random orientation effects.[25]

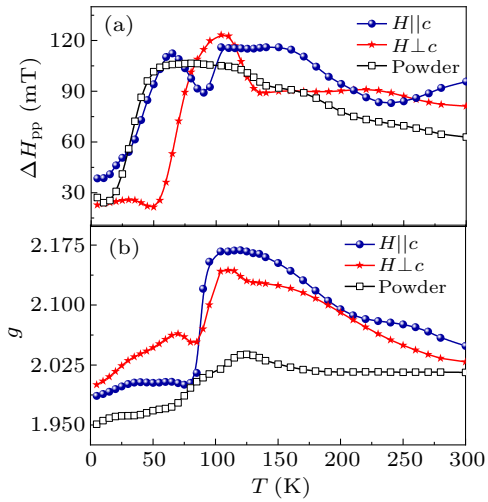



**Fig. 7.** (a)–(b) The temperature dependence of $\Delta H_{pp}$ and $g$ for powder and single crystal $Nb_3Cl_8$ with both $H \parallel c$ and $H \perp c$ orientations.

## 4. Conclusion

In this study, fine single crystals of the cluster magnet $Nb_3Cl_8$ were synthesized by the flux method and characterized using XRD, SEM, and EDS techniques. The local magnetic environment and anisotropic magnetism of cluster magnet were successfully probed using ESR spectroscopy. The non-magnetic transition has clearly observed in single crystal samples for both with $H \parallel c$ and $H \perp c$ at $T^* \sim 100$ K, evidenced by suppression of intensity $I$ trends. In contrast, the powder sample analysis reflects the averaging of anisotropic effects and absence of non-magnetic transition. Significant temperature dependence changes in $g$, $\Delta H_{pp}$, and $I$ highlighted the interplay between spin–orbit coupling, spin–spin interactions, and anisotropic magnetism in $Nb_3Cl_8$. These findings demonstrate ESR's sensitivity to probe the local spin dynamics at microscopic level. This work enhances our understanding of the local magnetic environment in single crystal of $Nb_3Cl_8$ and contribute to growing field of low-dimensional quantum materials, particularly applications in spintronics, quantum computing and tunable magnetic systems.

## Acknowledgement

Project supported by the National Natural Science Foundation of China (Grant Nos. 52088101, 12174425, and U23A20550).

## References

[1] Shi G, Huang N, Qiao J, Zhang X, Hu F, Hanwei H, Xinyu Z and Shang J 2024 *Nanomaterials* **14** 1759
[2] Zhang S, Xu R, Luo N and Zou X 2021 *Nanoscale* **13** 1398
[3] Goyal R and Goyal K 2025 *J. Mater. Sci. Mater. Eng.* **20** 4
[4] Wang Q H, Blei M, Hamo A, Jenkins S, Augustin M and Fert A 2022 *ACS Nano* **16** 6960
[5] Pasco C M, Baggari I E, Bianco E, Kourkoutis L F and McQueen T N 2019 *ACS Nano* **13** 9457
[6] Haraguchi Y, Michioka C, Ishikawa M, Nakano Y, Yamochi H, Ueda H and Yoshimura K 2017 *Inorg. Chem.* **56** 3483
[7] Cotton F A, Diebold M P and Roth W J 1987 *J. Am. Chem. Soc.* **109** 2833
[8] Haraguchi Y and Yoshimura K 2024 *J. Phys. Soc. Jpn.* **93** 111002
[9] Jiang Z, Jiang D, Wang Y, Li C, Liu K, Wen T, Liu F, Zhou Z and Wang Y 2022 *Sci. China Phys. Mech. Astron.* **65** 278211
[10] Liu B, Zhang Y, Han X, Sun J, Zhou H, Li C, Cheng J, Yan S, Lie H, Shi Y, Yang H and Li S 2024 *J. Phys.: Condens. Matter* **36** 155602
[11] Sheckelton J P, Plump K W, Trump B A, Broholm C L and McQueen T M 2017 *Inorg. Chem. Front.* **4** 481
[12] Sun Z, Zhou H, Wang C, Kumar S, Geng D, Yue X, Han S, Haraguchi Y, Shimanda K, Cheng P, Chen L, Shi Y, Wu K, Meng S and Feng B 2022 *Nano Lett.* **22** 4596
[13] Yoon J, Lesne E, Sklarek K, Sheckelton J, Pasco C, Parkin S S P, McQueen T M and Ali M N 2020 *J. Phys.: Condens. Matter* **32** 304004
[14] Zhang Y, Gu Y, Weng H, Jiang K and Hu J 2023 *Phys. Rev. B* **107** 035126
[15] Polash M M H, Smirnov A I and Vashaee D 2023 *Appl. Phys. Rev.* **10** 045004
[16] Freed J H and Fraenkel G K 1963 *J. Chem. Phys.* **39** 326
[17] Rieger P H 2007 *Electron Spin Resonance: Analysis and Interpretation* (Cambridge: RSC Publishing)
[18] Shchepetilnikov A V, Frolov D D, Nefyodov A Y, Kukushkin I V, Tiemann L, Reichl C, Dietsche W and Wegscheider W 2018 *Phys. Rev. B* **98** 241302
[19] Lund A, Shiotani M and Shimada S 2011 *Principles and Applications of ESR Spectroscopy* (Berlin: Springer)
[20] Taylor R 1975 *Adv. Phys.* **24** 681
[21] Causa M, Tovar M, Caneiro A, Prado F, Ibanez G, Ramus C A, Butera A, Alascio B, Obradors X and Pinol X 1998 *Phys. Rev. B* **58** 3233
[22] Do S H, Tol J V, Zhou H D and Choi K Y 2014 *Phys. Rev. B* **90** 104426
[23] Sheckelton J P 2015 *Strongly Correlated Molecular Magnetism in Triangular-Lattice Cluster Materials* (Baltimore: Johns Hopkins University)
[24] Adrian F J 1968 *J. Colloid Interface Sci.* **26** 317
[25] Hulliger J, Zoller L and Ammeter J H 1982 *J. Magn. Reson.* **48** 512
[26] Zorko A, Nellutla S, van Tol J, Brunel L C, Bert F, Duc F, Trombe J C, de Vries M A, Harrison A and Mendels P 2008 *Phys. Rev. Lett.* **101** 026405
[27] Lee B, Zhang X, Kang J, Jeong B J, Cho S, Choi K H, Jeon J, Lee S H, Kim D, Kim Y H, Kim J H, Yu H K and Choi J Y 2024 *Nanoscale* **16** 20312